Optics Letters

Miniature probe for *in vivo* optical- and acoustic-resolution photoacoustic microscopy

Zhendong Guo,[1] Yao Li,[1] and Sung-Liang Chen[1,2,*]

[1]University of Michigan-Shanghai Jiao Tong University Joint Institute, Shanghai Jiao Tong University, Shanghai 200240, China
[2]State Key Laboratory of Advanced Optical Communication Systems and Networks, Shanghai Jiao Tong University, Shanghai 200240, China
*Corresponding author: sungliang.chen@sjtu.edu.cn

Received 21 November 2017; revised 15 December 2017; accepted 31 January 2018; posted 2 February 2018 (Doc. ID 313981); published 28 February 2018

We present a miniature probe capable of both optical-resolution (OR) and acoustic-resolution (AR) photoacoustic microscopy. A gradient-index-lens fiber and a multimode fiber are used to deliver light for OR and AR illumination, respectively. The probe achieves lateral resolution of 3.1 μm for OR mode and 46–249 μm (at depth of 1.2–4.3 mm) for AR mode, respectively. The size of the probe attains 3.7 mm in diameter, which can be used for endoscopic applications. *In vivo* imaging of several different parts of a mouse demonstrates the excellent imaging ability of the probe.

OCIS codes: (170.5120) Photoacoustic imaging; (170.3880) Medical and biological imaging; (110.4190) Multiple imaging.

https://doi.org/10.1364/OL.43.001119

During the past few years, a variety of miniature probes for photoacoustic endoscopy (PAE), a novel endoscopic modality to image internal organs with minimal invasion, have been developed [1–13]. Photoacoustic microscopy (PAM) offers exceptional sensitivity to optical absorption contrast associated with a wealth of physiological or functional information [14], such as oxygen saturation of hemoglobin [15] and velocity of blood flow [16,17]. PAM can be classified into optical-resolution (OR) PAM (OR-PAM) and acoustic-resolution (AR) PAM (AR-PAM). The former uses a focused laser beam to achieve high lateral resolution at superficial tissue layers, while the latter employs a focused ultrasonic transducer to attain moderate lateral resolution for deep imaging up to several millimeters. Hence, PAM conducted in an endoscopic manner is of biomedical and medical significance and has demonstrated potential applications in cardiovascular [8,11], gastrointestinal [4,5,9], and urogenital systems [2,3]. Similarly, PAE can be classified into OR-PAE [3,6–9] and AR-PAE [4,5]. Currently, most developed PAE probes can only perform one mode. Integrating OR- and AR-PAE in a probe enables scalable resolution and depth. Although combined OR- and AR-PAM (OR-AR-PAM) systems with satisfactory *in vivo* imaging have been demonstrated [18–20], endoscopic applications are highly restricted due to the bulky size of the imaging heads. An imaging head of ≥6 mm in diameter capable of hybrid OR- and AR-PAM was reported [21], yet the size is still large compared with the 3.8 mm working channel of commercial video endoscopes. Another 3.6 mm probe was demonstrated [10]; however, the design yields relatively low lateral resolution of 13 μm and ~250 μm (at depth of 1.5 mm) for OR and AR, respectively. Moreover, only *ex vivo* imaging results with mediocre quality were showcased.

In this Letter, we design a 3.7 mm miniature probe capable of performing OR- and AR-PAM. Specifically, compared with the previous work [10], we accomplish high lateral resolution of 3.1 μm and 46–249 μm (at depth of 1.2–4.3 mm) for OR and AR, respectively, which is comparable to bulky OR- and AR-PAM systems. Furthermore, *in vivo* imaging with excellent image quality is demonstrated.

Figure 1(a) shows the schematic of the OR- and AR-PAE (OR-AR-PAE) probe. A custom-made hollow focused transducer (OPTOSONIC Inc., San Gabriel, CA) with a center frequency of 45 MHz, an acoustic focal length of 4.2 mm, an inner diameter (ID) of 0.9 mm, and an outer diameter (OD) of 2.8 mm is used for acquiring photoacoustic signals. The −6 dB depth of focus of the transducer's acoustic detection focal volume is 1.5 mm, as calibrated experimentally using a photoacoustic object (a black tape). A single-mode fiber (SMF) (P1-460B-FC-2, Thorlabs) and twin gradient-index (GRIN) lenses (GT-LFRL-050-023-50-CC (532), GRINTECH) were assembled together with a glass tube (ID: 0.55 mm; OD: 0.85 mm) to form a GRIN-lens fiber for OR illumination. The equivalent numerical aperture (NA) of the twin GRIN lenses with a proper design can be larger than the NA of one single GRIN lens. Thus, lateral resolution can be enhanced by using the twin GRIN lenses. The details will be presented in another work. For AR illumination, a multimode fiber (MMF) (MM-S105/125-22A, Nufern) with a core diameter of 105 μm and NA of 0.22 was aligned with the transducer's acoustic detection focal volume at a tilt angle of 20 degrees. Note that a custom-made acrylic holder with a wedge-shaped distal end is used to bend the MMF to have the desired tilt angle. The OR illumination focus, the acoustic detection focal volume, and the AR illumination zone can be adjusted by the GRIN-lens fiber, the transducer, and the MMF, respectively. Specifically, the OR illumination focus can be adjusted by moving the

GRIN-lens fiber before assembling it with the acoustic transducer. The focal lengths of the GRIN-lens fiber and the acoustic transducer are known (measured beforehand). By checking the delay time of the acquired photoacoustic signal, the relative position of the OR illumination focus and the acoustic detection focus can be obtained. On the other hand, different tilt angles of the MMF can be adjusted by a rotation stage during the development and testing phase. By checking the acquired photoacoustic signal from the sample at different depths, the imaging depth range can be measured. OR mode is expected to acquire images at a depth within 1 mm from the surface of biological tissue, while AR mode is for depths larger than 1 mm. Although a confocal arrangement of the OR focus and acoustic focus offers the best sensitivity for OR mode, in this way, the region that is relatively far from the acoustic focus will be mainly used for AR mode, which sacrifices the sensitivity and imaging depth range for AR mode. Thus, to balance the OR-PAM sensitivity, AR-PAM sensitivity, and AR-PAM imaging depth range, the arrangement in Fig. 1(b) is used. As shown in Fig. 1(b), the current working distance is 1.4 mm due to the GRIN-lens fiber. The working distance can be further extended at the expense of OR resolution. To improve resolution and sensitivity of AR-PAM images in the out-of-focus region of the transducer, synthetic aperture focusing technique (SAFT) and coherence factor (CF) are used [22]. Figure 1(c) shows the photograph of the probe, which has an overall size of 3.7 mm in diameter and can be readily inserted through working channels of commercial endoscopes.

Figure 1(d) shows the imaging system for the OR-AR-PAE probe. OR Illumination is provided by a 532 nm pulsed laser (FDSS532-Q3, CryLas) with a high repetition rate (maximum: 2.5 kHz), and AR illumination is provided by another 532 nm pulsed laser (Spitlight DPSS EVO I, InnoLas) with high laser energy per pulse. Both lasers are attenuated, spatially filtered, and coupled to the SMF and the MMF for OR and AR illumination, respectively. Note that the AR illumination at other wavelengths such as near infrared (IR) can also be delivered by the MMF. The laser fluence at the surface of the sample is 27–41 mJ/cm^2 for OR-PAM and ~7 mJ/cm^2 for AR-PAM. The photoacoustic signals without averaging are amplified by a preamplifier (ZFL-500LN-BNC+, Mini-Circuits) and sampled by a high-speed digitizer (CSE1422, Gage) with sampling rate of 200 MS/s and 14-bit resolution. The acrylic holder of the OR-AR-PAE probe is mounted on a two-dimensional (2D) motorized stage [M-404, Physik Instrumente (PI)] for scanning during image acquisition. In our current system, 2D linear scans are performed to obtain volumetric images to demonstrate the imaging ability of the probe. In practical and clinical endoscopic imaging applications, rotational scanning ability can be realized by using a micromotor in the future [1,4,5,9].

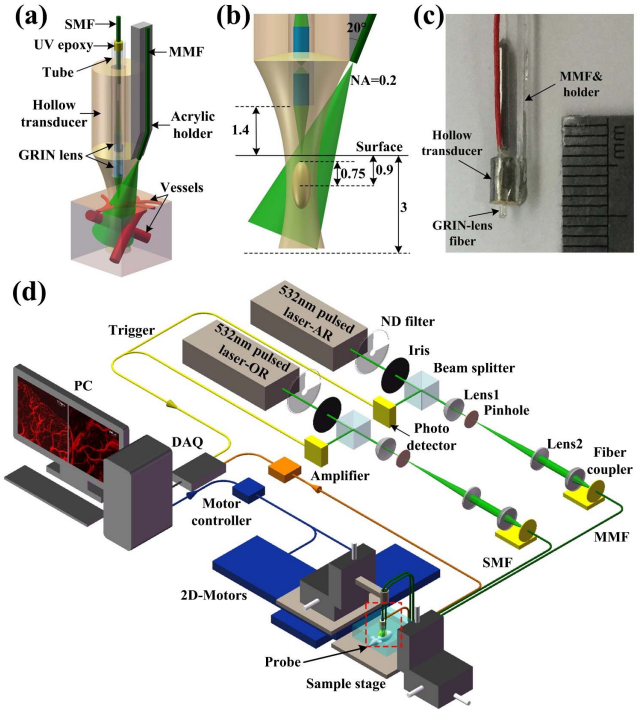

Fig. 1. (a) Schematic of the OR-AR-PAE probe. (b) Arrangement of OR and AR illumination; unit length, mm. (c) Photograph of the OR-AR-PAE probe. (d) Schematic of the imaging system for the probe; ND, neutral density; PC, personal computer.

To characterize the OR-AR-PAE probe, we imaged different phantoms for complete calibration. To measure the OR resolution, the edge of a sharp blade was imaged by OR-PAM. Figure 2(a) presents the OR-PAM image in one dimension and its curve fitting by the edge-spread function (ESF). By taking the first derivative of the ESF, a line-spread function (LSF) was obtained, and the OR resolution can be estimated by the full width at half maximum (FWHM) of the LSF. As shown in Fig. 2(a), OR resolution of 3.1 μm is achieved, which is similar to conventional benchtop OR-PAM systems. On the other hand, to quantify the AR resolution as well as its imaging depth, a phantom composed of five tungsten wires 18 μm in diameter was imaged by the OR-AR-PAE probe. The positions of tungsten wires along x

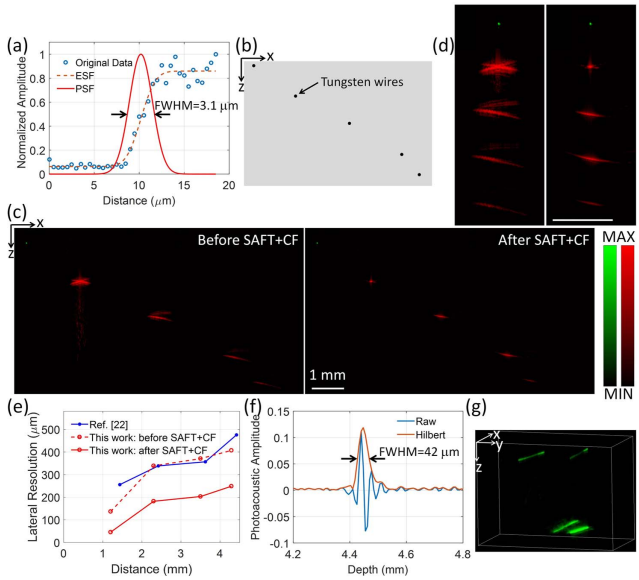

Fig. 2. (a) Calibrated OR lateral resolution. (b) Schematic illustration of tungsten wire phantom. (c) Fused OR- and AR-PAM images before and after SAFT and CF. The scale bar is for both images. The green and red color bars are for OR- and AR-PAM images with dynamic ranges of 15 dB and 40 dB, respectively. (d) Zoom images of (c) before SAFT and CF (left) and after SAFT and CF (right) for better visualization. The scale bar is 1 mm for both images. The imaged contrasts from top to bottom correspond to those from top to bottom in (c). (e) Calibrated AR lateral resolution (in comparison with Ref. [10]). (f) Measured axial resolution. (g) 3D OR-PAM and AR-PAM of another tungsten wire phantom.

(lateral) and z (depth) directions are illustrated in Fig. 2(b). Figure 2(c) shows the OR (in green color) and AR (in red color) images (before and after SAFT and CF) where the top wire was imaged by OR-PAM and the rest by AR-PAM. The OR-PAM image is able to visualize the shallow tungsten wire at high resolution, while the AR-PAM image can image much deeper at moderate resolution. For better visualization, zoom images of Fig. 2(c) are presented in Fig. 2(d). The FWHMs of the imaged tungsten wires are checked to quantify the AR resolution. It is found that the AR resolution is improved from 137, 339, 371, and 407 μm to 46, 182, 203, and 249 μm, at depths of 1.2, 2.3, 3.5, and 4.3 mm, respectively, after applying SAFT and CF. From the imaged size of 46–249 μm, the 18-μm tungsten wires can still be considered as a good approximation of a point source, although a smaller sample (e.g., 6 μm carbon fibers) can better approach the AR resolution. As shown in Fig. 2(e), our AR resolution (after SAFT and CF) is much better than that reported in Ref. [10], where the filtered back-projection method is used [10]. The relatively low AR resolution at the out-of-focus region of the transducer after SAFT and CF is mainly due to the low NA of the MMF. The out-of-focus AR resolution can be improved by using a large-NA MMF for AR illumination. The axial resolution is provided by the acoustic bandwidth of the transducer, and thus, OR- and AR-PAM share the same axial resolution. The envelope of the photoacoustic A-line signal from the tungsten wire has a FWHM of 42 μm, as shown in Fig. 2(f). Thus, the axial resolution is better than 42 μm. To demonstrate the volumetric imaging ability of the OR-AR-PAE probe, another phantom composed of four 18 μm tungsten wires with two placed at the surface and two at a depth of ~2 mm was imaged. Figure 2(g) depicts the three-dimensional (3D) image, where the top two wires were imaged by OR-PAM and the bottom two by AR-PAM, which shows again the complementary nature of OR-PAM for high resolution and AR-PAM for deep imaging.

To assess the *in vivo* imaging performance of the OR-AR-PAE probe, different parts of a mouse were imaged by OR-PAM or AR-PAM. All experimental animal procedures were carried out in conformity with the laboratory animal protocol approved by Laboratory Animal Care Committee of Shanghai Jiao Tong University. The mouse was anesthetized with pentobarbital and placed on an animal platform. For *in vivo* OR-PAM demonstration, we imaged the mouse ear and eye. The mouse ear is a thin tissue (<1 mm), and the mouse eye has microvessels mainly in the superficial layer. Therefore, OR-PAM is more suitable to image the two parts. A large area of 3.92 × 3.4 mm^2 of the mouse ear was imaged by OR-PAM, as shown in the maximum amplitude projection (MAP) image in Fig. 3(a), which clearly shows the vascular network over almost the whole ear. A small zoom region of 1 × 1 mm^2 [white dashed box in Fig. 3(a)] around the rim of the ear was imaged, as shown in Fig. 3(b). Due to the high resolution, more details including capillaries are better visualized. Another small zoom region [white dashed box in Fig. 3(b)] is shown in Fig. 3(c), where single red blood cells (RBCs) can be identified. Figure 3(d) shows the OR-PAM image of the mouse eye, where a radial distribution of blood vessels from the pupil is observed.

On the other hand, for *in vivo* AR-PAM demonstration, the mouse dorsal part and leg were imaged. Since the two sites have relatively more subcutaneous blood vessels at certain depths, AR-PAM is more favorable and can be acquired by the same OR-AR-PAE probe. As shown in Fig. 4(a), a region of 11.4 × 11.3 mm^2 on the back of a mouse was imaged *in vivo*. Considering the same size of imaging areas, the AR-PAM image presents fewer blood vessels compared with the OR-PAM images in Fig. 3. However, the AR-PAM image is able to reveal large blood vessels that reside in deep tissues, which cannot be manifested by OR-PAM. As shown in Fig. 4(b), a representative B-mode image shows that AR-PAM can image at a depth up to 2.07 mm. Figure 4(c) shows the whole mouse leg over a large area of 24 × 27.2 mm^2 imaged by AR-PAM, and a representative B-mode image [Fig. 4(d)] shows again the deep imaging ability of AR-PAM. Note that the 532 nm laser illumination was used in this demonstration. Imaging depth can be further extended, and more vessels at depth can be visualized by using near-IR laser illumination.

Currently, the MMF with low NA of 0.22 is used, which results in a smaller laser illumination extent than the acoustic detection angular extent in the out-of-focus region, especially for the region far from the acoustic focus. Since photoacoustic signals are generated from smaller angular extent, the resolution restoration after SAFT and CF is discounted. The issue can be solved by using a large-NA MMF for AR illumination to ensure a larger laser illumination extent than the acoustic detection angular extent in the out-of-focus region. In this way, the out-of-focus AR resolution can be better restored.

To realize rotational scanning ability for practical and clinical endoscopic imaging applications, a micromotor can be used in the future [1,4,5,9]. The arrangement of OR and AR illumination in the original design (without a micromotor) is applicable to the probe with a micromotor for side-view imaging. A pull-back rotary scan can be performed to realize 3D imaging. For side-view OR-PAM, the working distance of the GRIN-lens fiber (currently 1.4 mm) should be extended to be at least larger than the radius of the side-view probe. The GRIN-lens fiber can be made with improved working distance but at the expense of OR resolution. Thus, further development of the GRIN-lens fiber to optimize the resolution and working distance is needed. For side-view AR-PAM, SAFT and

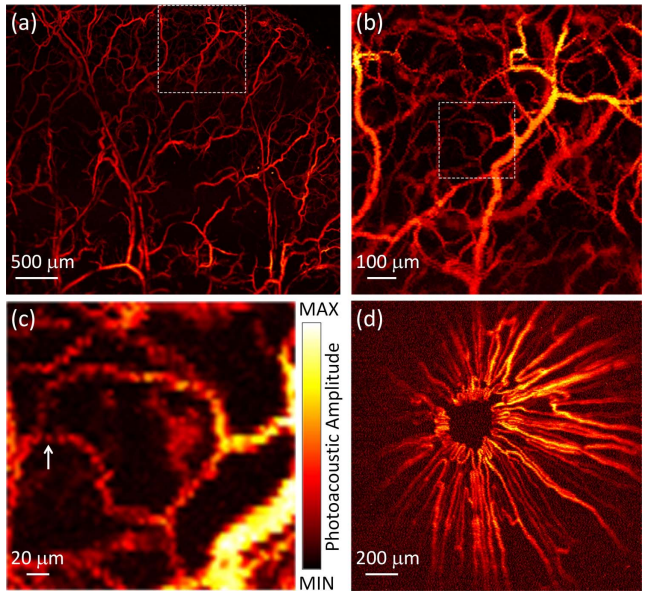

Fig. 3. (a) OR-PAM (MAP) of mouse ear. (b) OR-PAM (MAP) of the zoom region in the white dashed box in (a). (c) OR-PAM (MAP) of the zoom region in the white dashed box in (b); the arrow indicates single RBCs. (d) OR-PAM (MAP) of mouse eye. The color bar is for images (a)–(d).

CF can be applied for improving the out-of-focus axial resolution (i.e., z axis in the cylindrical coordinate system) by linear scan along the axial direction. On the other hand, SAFT and CF can also be applied for enhancing the out-of-focus transverse resolution, as detailed in Ref. [12].

In summary, we proposed and constructed a miniature OR-AR-PAE probe and demonstrated its *in vivo* imaging of different parts of a mouse. The probe has a diameter of 3.7 mm and thus can readily fit in the working channel of a white-light endoscope. Table 1 shows the comparison of all existing integrated OR-AR-PAM systems, to our knowledge. First, the benchtop systems have high OR and AR resolutions but are not suitable for endoscopic applications [18–20]. Second, the probe in Ref. [21] has low OR and AR resolutions and a diameter of >6 mm, which is still too large for endoscopy. Third, the probe in Ref. [10] reaches a diameter of 3.6 mm, which had been the smallest OR-AR-PAE probe. However, the probe suffered from relatively low OR and AR resolutions, and only *ex vivo* imaging results with mediocre quality were demonstrated. In contrast to other existing OR-AR-PAM works [10,18–21], the novelty of this Letter lies in two parts: (a) high OR and AR resolutions comparable to the benchtop systems are achieved while the probe size is kept similar to a minimum so far [10]; (b) high-quality *in vivo* imaging of several different parts of a mouse manifests the comparable imaging ability to the benchtop systems. Note that other wavelengths such as near IR can be delivered by the MMF to enable deeper and/or functional imaging. In addition to endoscopic applications, the demonstrated OR-AR-PAE probe also serves as a simple alternative to benchtop OR-PAM and AR-PAM imaging heads.

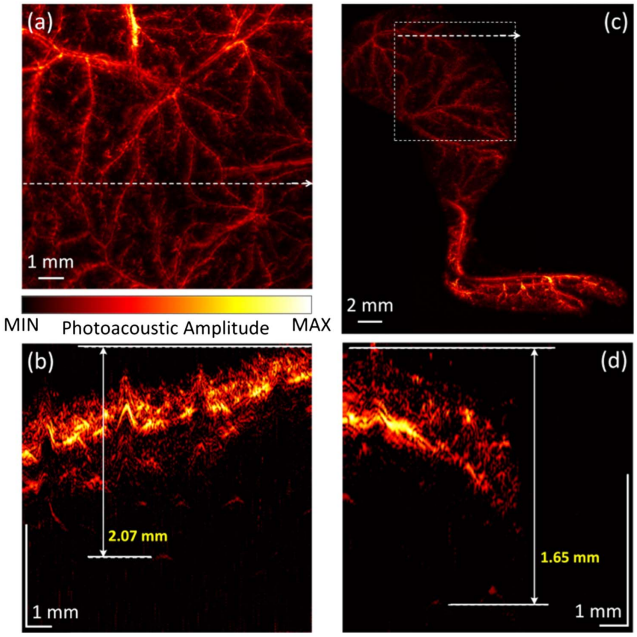

Fig. 4. (a) AR-PAM (MAP) of mouse back. (b) B-mode image (dynamic range: 33 dB) along the white dashed line in (a). (c) AR-PAM (MAP) of mouse leg. (d) B-mode image (dynamic range: 30 dB) along the white dashed line in (c). The color bar is for images (a) and (c). (d) 3D volume rendering US image. 3D animations are available as supplementary videos: 3D volume rendering photoacoustic images of the mouse back in (a) (Visualization 1) and the mouse leg in (c) where the white dashed box region is selected (Visualization 2). Near-IR laser illumination can be used for deeper imaging.

Table 1. Comparison of Integrated OR- and AR-PAM

Refs.	Probe Size (mm)	Lateral Resolution (μm) OR	AR	Demonstration
[18]	bulky	2.2	40	*in vivo* mouse ear and back
[19]	bulky	2.5	80	*in vivo* mouse ear, eye, brain, and leg
[20]	bulky	4.2	45	*in vivo* mouse ear
[21]	>6	21	139	*in vivo* mouse brain
[10]	3.6	13	250[a]	*ex vivo* mouse ear
This Letter	3.7	3.1	46–249[b]	*in vivo* mouse ear, eye, back, and leg

[a]At depth of 1.5 mm.
[b]At depth of 1.2–4.3 mm [also see Fig. 2(e)].

Funding. National Natural Science Foundation of China (NSFC) (61405112, 61775134); National High Technology Research and Development Program of China (863 Program), Ministry of Science and Technology of the People's Republic of China (MOST) (2015AA020944).

REFERENCES

1. J.-M. Yang, K. Maslov, H.-C. Yang, Q. Zhou, K. K. Shung, and L. V. Wang, Opt. Lett. **34**, 1591 (2009).
2. Y. Yang, X. Li, T. Wang, P. D. Kumavor, A. Aguirre, K. K. Shung, Q. Zhou, M. Sanders, M. Brewer, and Q. Zhu, Biomed. Opt. Express **2**, 2551 (2011).
3. S.-L. Chen, Z. Xie, T. Ling, L. J. Guo, X. Wei, and X. Wang, Opt. Lett. **37**, 4263 (2012).
4. J.-M. Yang, R. Chen, C. Favazza, J. Yao, C. Li, Z. Hu, Q. Zhou, K. K. Shung, and L. V. Wang, Opt. Express **20**, 23944 (2012).
5. J.-M. Yang, C. Favazza, R. Chen, J. Yao, X. Cai, K. Maslov, Q. Zhou, K. K. Shung, and L. V. Wang, Nat. Med. **18**, 1297 (2012).
6. L. Xi, C. Duan, H. Xie, and H. Jiang, Appl. Opt. **52**, 1928 (2013).
7. B. Dong, S. Chen, Z. Zhang, C. Sun, and H. F. Zhang, Opt. Lett. **39**, 4372 (2014).
8. X. Bai, X. Gong, W. Hau, R. Lin, J. Zheng, C. Liu, C. Zeng, X. Zou, H. Zheng, and L. Song, PLoS One **9**, e92463 (2014).
9. J.-M. Yang, C. Li, R. Chen, B. Rao, J. Yao, C.-H. Yeh, A. Danielli, K. Maslov, Q. Zhou, K. K. Shung, and L. V. Wang, Biomed. Opt. Express **6**, 918 (2015).
10. H. He, G. Wissmeyer, S. V. Ovsepian, A. Buehler, and V. Ntziachristos, Opt. Lett. **41**, 2708 (2016).
11. X. Dai, H. Yang, T. Shan, H. Xie, S. A. Berceli, and H. Jiang, ACS Photon. **4**, 174 (2017).
12. D. Cai, G. Li, D. Xia, Z. Li, Z. Guo, and S.-L. Chen, Opt. Express **25**, 20162 (2017).
13. G. Li, Z. Guo, and S.-L. Chen, Opt. Express **25**, 25023 (2017).
14. J. Yao and L. V. Wang, Laser Photon. Rev. **7**, 758 (2013).
15. Y. Wang, S. Hu, K. Maslov, Y. Zhang, Y. Xia, and L. V. Wang, Opt. Lett. **36**, 1029 (2011).
16. J. Yao, K. I. Maslov, Y. Zhang, Y. Xia, and L. V. Wang, J. Biomed. Opt. **16**, 076003 (2011).
17. S.-L. Chen, Z. Xie, P. L. Carson, X. Wang, and L. J. Guo, Opt. Lett. **36**, 4017 (2011).
18. W. Xing, L. Wang, K. Maslov, and L. V. Wang, Opt. Lett. **38**, 52 (2013).
19. S. Jeon, J. Kim, and C. Kim, Proc. SPIE **9708**, 970845 (2016).
20. M. Moothanchery and M. Pramanik, Sensors **17**, 357 (2017).
21. H. Estrada, J. Turner, M. Kneipp, and D. Razansky, Laser Phys. Lett. **11**, 045601 (2014).
22. D. Cai, Z. Li, Y. Li, Z. Guo, and S.-L. Chen, Opt. Express **25**, 1421 (2017).